Crystallization of nanoheterogeneities in Ga-containing germanosilicate glass: dielectric and refractive response changes

A. Paleari,[ab] V.N. Sigaev,[a] N.V. Golubev,[a] E.S. Ignat'eva,[a] S. Bracco,[b] A. Comotti,[b] A. Azarbod,[bc] R. Lorenzi[b]*

a. P.D. Sarkisov International Laboratory of Glass-based Functional Materials, Mendeleev University of Chemical Technology of Russia, Miusskaya Square 9, 125190 Moscow, Russia

b. Department of Materials Science, University of Milano-Bicocca, Via R. Cozzi 55, 20125 Milano, Italy

c. Department of Physics, University of Ferrara, Via Saragat 1, 44100 Ferrara, Italy

** Corresponding author:* alberto.paleari@unimib.it

Abstract

Modification of the optical and dielectric response upon nanocrystallization represents a tool for functionalizing glass-based materials and an alternative approach for data storage in optical media. Here we report results for Ga-containing alkali-germanosilicate glass undergoing thermally activated secondary phase separation and crystallization of native nanoheterogeneities with formation of dense dispersions (105 μm^{-3}) of γ-Ga_2O_3 nanocrystals in transparent glass ceramics. The shift of the Urbach tail in the UV absorption and the refractive index increase upon nanocrystallization are analyzed following Duffy's approach and the Maxwell–Garnett description of refractive index in composite systems. The results clarify that native nanoheterogeneities consist of Ge-containing Ga-oxide and, consequently, composition changes occur between matrix and nanophase during nanocrystallization. Complex impedance data are analyzed to disentangle the electronic and ionic contributions to the dielectric response, pointing to a lowering of ionic polarizability parallel to the electronic polarizability increase. The analysis, aided by 71Ga NMR data, gives an insight into the relation between coordination changes and refractive and dielectric response, highlighting the role of non-bridging-oxygens and interphase.

Keywords: Amorphous oxides; Crystalline nanostructure; Optical spectroscopy

1. Introduction

The optical and dielectric functions of wide-band-gap mixed glasses are usually tuned by choosing appropriate compositions and doping. Any change in the mean coordination structure is in fact

accompanied by changes in the material polarization in response to electromagnetic radiation [1], [2]. However, the physical properties of an optical glass sometimes need to be efficiently controlled, at fixed macroscopic composition, on the very local scale of micrometer-sized patterns. In fibre optics, for instance, refractive index patterns are created from processes of laser-induced local densification, creation or release of local stresses, photoconversion of coordination defects, nanocrystallization and even amorphization of pre-existent crystalline nanophases [3], [4], [5], [6], [7]. Similar modifications can also constitute the fundamental ingredient for the development of novel optical memories with unprecedented storage capacity and stability, as recently envisaged and proved on glass systems [8], [9]. All these mechanisms are based on the intrinsic structural metastability of the amorphous network of glasses, which confers on glass-based materials a wide range of structural configurations and consequent possible transformations, including nanostructuring. Mechanisms of structural perturbation can comprise changes in the mean coordination number or coordination ring order (as in photosensitive germanosilicates and tin silicates [5]), chemical reactions of embedded components (as in fluorine-containing sol–gel silica [10]) and nucleation of crystalline nanophases. The latter class of processes is particularly interesting if nanostructure size and refractive index can be controlled so as to preserve optical transmittance, as in SnO_2-doped silica and Ga-containing glasses [11], [12].

The addition of gallium oxide can be a powerful tool for introducing additional degrees of freedom into the coordination structure of glasses, since Ga^{3+} ions admit very different coordination shells, from tetrahedral to octahedral ones, and compatibility both with amorphous networks and crystalline structures [12], [13], [14], [15]. These features make it possible to obtain Ga-modified germanosilicates in a fully amorphous form that can be drawn into fibres and functionalized by post-synthesis thermal or laser treatments of nanocrystallization [16], [17], [18]. This peculiarity was used to obtain Ga-oxide nanocrystals in glass as a suitable host for light-emitting ions [14], [15], [16], [17]. In such a case, it was also demonstrated that nanocrystals are the result of a secondary phase separation from native amorphous nanoheterogeneities in the glass and give rise to strong UV-excited visible light emission [19], [20]. However, no detailed information is available on the local changes in the structure and coordination occurring in the material, and on the relationships between the dielectric and refractive properties.

Here we report for the first time, to the best of our knowledge, detailed identification of the changes in polarization induced by nanostructuring an oxide glass. Specifically, in the present case, we report the analysis of Ga-modified germanosilicate glass undergoing thermally induced formation of γ-Ga_2O_3 nanocrystals. We present data and analysis which offer the possibility of controlling and tailoring the mean coordination structure of Ga-containing germanosilicate glasses for specific applications, particularly for designing processes of material patterning and functionalization.

2. Experimental procedure

Glass with nominal composition $7.5Li_2O$-$2.5Na_2O$–$20Ga_2O_3$–$35GeO_2$–$35SiO_2$ (mol.%) was prepared by a conventional melt-quenching method. The raw materials are Li_2CO_3 (reagent grade), Na_2CO_3 (reagent grade), Ga_2O_3 (reagent grade), GeO_2 (special purity grade) and amorphous SiO_2 (special purity grade). A Ga-free reference sample, with the other oxide components in unchanged proportions, was also prepared by the same procedure. In all cases, the amount of reagent in each batch was calculated in order to prepare 120 g of final product. The starting materials were weighed using an analytical balance with an accuracy of 0.001 g and carefully mixed in an agate mortar. Glass was then prepared in a 45 ml crucible in air at 1480 °C for 40 min. Final glass samples were analyzed by energy-dispersive X-ray fluorescence analysis (Bruker Artax 200), verifying the absence of contaminants down to the detection limit of a few ppm. A fraction of as-quenched bulk samples were heat treated at about 690 °C for 15 min, in order to induce nanocrystallization, by putting the glass samples into a muffle furnace in air with a temperature accuracy of ±2 K, with initial and final transients of the order of a few seconds. The densities of all materials were determined through hydrostatic measurements with an uncertainty of less than 1%. Compositions, molar mass, density and calculated molar volume of the investigated materials are summarized in Table 1. Samples were then obtained from the final materials either as polished slabs or powders according to the type of measurement to be performed.

Material	Composition	Density	M_M	V_M
AQ	7.5 2.5 20.0 35.0 35.0	3.655	98.9279	27.07
TT	7.5 2.5 20.0 35.0 35.0	3.662	98.9279	27.01
GF	9.4 3.0 0.00 43.8 43.8	3.189	76.8166	24.09

Table 1. Material data. Nominal composition (molar percentage of Li_2O, Na_2O, Ga_2O_3, GeO_2, and SiO_2, respectively), density (g cm^{-3}), molar mass M_M (g mol^{-1}) and molar volume V_M (cm^3 mol^{-1}) of as-quenched glass (AQ), thermally treated nanostructured glass (TT) and Ga-free reference glass (GF). Uncertainty in the density and molar volume is 0.3%.

Transmission electron microscopy (TEM) images and electron diffraction patterns were obtained on finely ground powder, deposited on a gold microscopy grid, using a FEI Tecnai G2 F20 field emission gun transmission electron microscope, with an accelerating voltage of 200 kV and equipped with an S-Twin lens that gives a point resolution of 0.24 nm. The imaging system is composed of one TV rate 626 Gatan and one slow scan 794 Gatan charge-coupled-device (CCD) camera. No effect of electron irradiation on the nanostructured materials was observed during low-resolution TEM measurements. Differential scanning calorimetry (DSC) measurements were performed by means of a Netzsch DSC 449F3 high-temperature thermoanalyzer in platinum crucibles, at a heating rate of 10 K min^{-1} in Ar, on bulk samples of 10–15 mg. X-ray diffraction (XRD) patterns of the powdered samples were recorded on a Bruker D2 PHASER diffractometer (Cu Kα radiation, Ni filter). Crystalline phases were identified by comparing positions and relative intensities of peaks in XRD patterns with data in the JCPDS (Joint Committee on Powder Diffraction Standards) database. Particular attention was paid to the preparation of samples for XRD estimation of the crystallized volume fraction, mainly as regards powder granulometry and positioning, so as to ensure a reliable semiquantitative comparison among distinct measurements. The 71Ga solid-state nuclear magnetic resonance (NMR) spectra were run at 91.5 MHz on a Bruker Avance 300 instrument operating at a static field of 7.04 T equipped with 4 mm double resonance magic angle spinning (MAS) probe. The samples were

spun at the magic angle and at a spinning speed of 16.5 kHz. A spin–echo sequence (90 °–τ–180°) was applied with a recycle delay of 10 s and the echo delay was set to the reciprocal of the MAS frequency. The MAS spectra were referenced to a 1 M aqueous solution of gallium nitrate and a 90° pulse of 3 μs was applied.

Optical absorption measurements were collected by means of a Perkin Elmer Lambda 9000 spectrophotometer with a cryostat for measurement down to 15 K with an uncertainty of ±1 K. The effects due to light reflection and scattering by the surfaces in optical absorption spectra are estimated from combined measurements of transmittance and diffused reflectance by means of an integrating sphere. Refractive index measurements were performed by a prism coupling refractometer Metricon 2010 working at 633 nm with an uncertainty lower than 10^{-3}. Fluorescence measurements were performed with a Dilor Labram spectrometer using a 632.817 nm He–Ne laser as a light source. Spectra were collected in backscattering geometry using a 50× objective with a spot radius of about 2 μm and a detection system with a CCD detector and a final spectral resolution of about 1 cm^{-1} (0.05 nm). Gold electrodes of approximately 1 cm^2 were deposited on the sample surfaces by sputtering for the characterization of the dielectric response. Complex impedance measurements were carried out in the 10^2–10^6 Hz range by means of a HP4284A impedance bridge. Values of relative electric permittivity $\in r(\nu)$ were determined from capacitance obtained from the imaginary part of complex impedance, electrode area and sample thickness, and normalizing for the vacuum permittivity $\in 0$. Similarly, from the geometrical parameters, the real part of impedance data was used to calculate the electrical conductivity $\sigma(\nu)$.

3. Results and discussion

3.1. Nanoheterogeneities and nanocrystals

In Fig. 1 we show a representative TEM image and electron diffraction pattern of nanostructured glassceramic material from Ga-modified alkali germanosilicate after thermal treatment. As recently demonstrated [12], [14], [15], gallium oxide segregates as homogeneously dispersed γ-Ga_2O_3 nanocrystals from native nanometer-sized heterogeneities, slightly smaller than 10 nm, evidenced in small-angle-

neutron-scattering (SANS) data [19]. Such heterogeneities occur in Ga-containing germanosilicates as a result of a liquid–liquid phase separation, but no indication of their composition has been collected up to now. Secondary phase separation of the native nanoheterogeneities is then induced by post-synthesis thermal treatments, giving rise to γ-Ga_2O_3 nanocrystals in the glass.

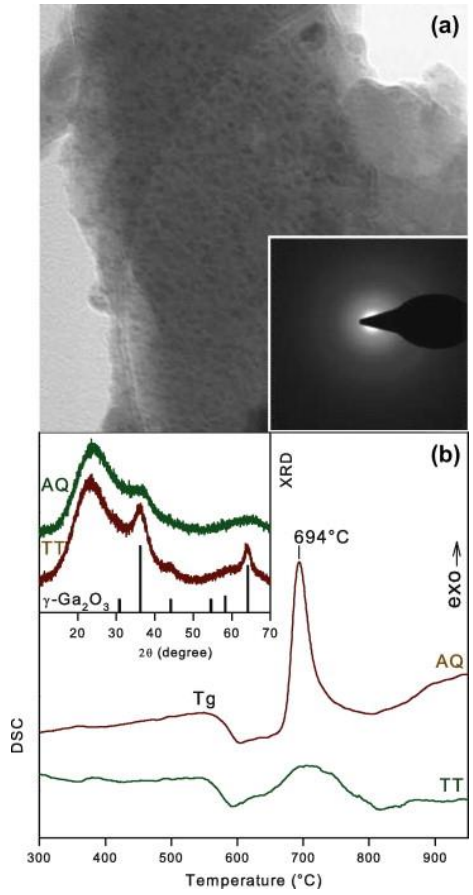

Fig. 1. (a) Electron microscopy image of Ga-containing 7.5Li_2O–2.5Na_2O–20Ga_2O_3–35GeO_2–35SiO_2 glass after 15 min of treatment at 690 °C. Inset: electron diffraction pattern. (b) Differential scanning calorimetry curves of as-quenched (AQ) glass (with evidence of an exothermic peak of γ-Ga_2O_3 crystallization) and 15 min treated sample (TT) in which the lack of a crystallization peak demonstrates almost full completion of the process after the first treatment. Inset: XRD patterns of the same glass before and after 15 min treatment, compared with expected positions of the γ-Ga_2O_3 reflections (sticks).

The TEM image in Fig. 1a shows nanocrystals formed after 15 min at 690 °C. This temperature falls into the exothermic peak observed in DSC measurements, as reported in Fig. 1b. After such a thermal treatment,

the nanophase consists of γ-Ga_2O_3 nanocrystals with a mean diameter of 6 ± 2 nm. The XRD pattern of the material after thermal treatment (inset in Fig. 1b) registers quite broad peaks, indicators of a nanosized crystalline phase. The linewidth of the peaks suggests crystalline domains of few nanometers, of the same order of the nanocrystal size estimated from TEM analysis. The comparison between XRD patterns before and after thermal treatment can be used to obtain an estimation of the amount of segregated crystalline phase. The comparative analysis of the broad halo of the amorphous matrix and the Bragg reflections of the crystalline nanophase after different treatment time (from 15 min to more than 100 h) gives evidence that the segregation of Ga_2O_3 crystalline phase can proceed up to completion [19]. The complete disappearance of the exothermic DSC peak after prolonged treatment supports the latter evaluation, since it is related to the completion of the Ga_2O_3 nanocrystallization process. In such a case, the volume fraction of the crystalline phase turns out to be consistent with the segregation of the major part of the entire content of Ga-oxide in the material, with an upper limit value slightly greater than 20% accounting for the larger molar volume of Ga-oxide with respect to Si- and Ge-oxides. Interestingly, the XRD pattern before thermal treatment shows that the substantially amorphous system cannot, however, be described as a homogeneous glass. The composite halo in the XRD pattern (comprising a secondary structure just below 2θ=40°) is indeed consistent with the occurrence of a separated phase, as in other nanostructured glasses and alloys [21], [22], [23] and also evidenced by SANS measurements [19]. Nevertheless, XRD data suggests a negligible domain of crystallinity, consistent with the absence of any crystalline feature in TEM analysis before thermal treatment. Therefore, even though the material turns out to be nanostructured both before and after thermal treatment, the structure and perhaps the composition do not remain unperturbed by the treatment. Since the final nanostructures consist of γ-Ga_2O_3 nanocrystals—with Ga^{3+} ions in both tetrahedral and octahedral sites—the transformation likely involves an increase of Ga^{3+} coordination number, which should be closer to 4 in the starting amorphous nanoheterogeneities, according to Zachariasen's criterion [24].

Clear-cut evidence of nanocrystallization-induced effects on the Ga^{3+} coordination number comes from NMR data. In Fig. 2 we report 71Ga MAS NMR spectra of $7.5Li_2O–2.5Na_2O–20Ga_2O_3–35GeO_2–35SiO_2$ before and after treatment at the crystallization temperature of 690 °C for 15 min. According to previous studies

on α-Ga_2O_3 (whose structure admits GaO_6 coordination only) and β-Ga_2O_3 (in which both GaO_6 and GaO_4 coordinations occur) [25], [26], [27], the chemical shift is expected to be strictly correlated with the coordination number. More specifically, the chemical shift is approximately 50–60 ppm in 6-fold coordinated GaO_6 sites, and more than 100 ppm in 4-fold coordinated GaO_4 sites [27]. The spectra in Fig. 2 register a significant modification of the signal shape upon nanocrystallization. Importantly, even though the overall signal shape is largely determined by the huge broadening caused by the heterogeneity of the sites, an intensity increase is clearly detected after treatment in the upfield region of the signal pattern at about 50 ppm. Such a change supports, as expected, a larger concentration of ordered 6-fold coordinated Ga sites in the nanocrystallized material [26]. Interestingly, a weak shoulder is detectable even in as-quenched glass, pointing to a non-negligible amount of GaO_6 sites in the initial glass.

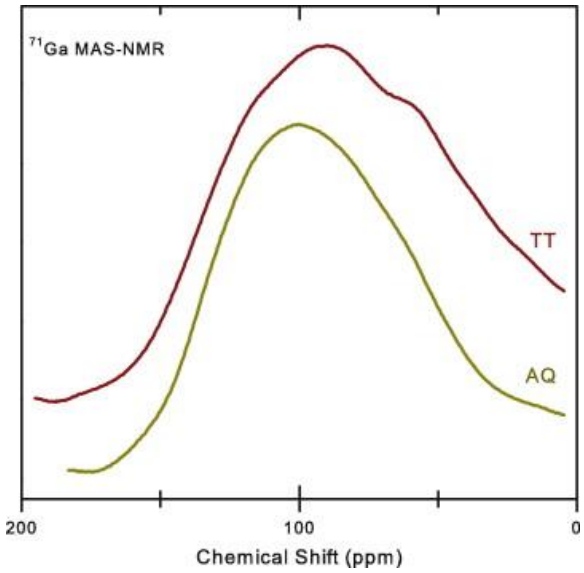

Fig. 2. 71Ga MAS NMR spectra of 7.5Li_2O–2.5Na_2O–20Ga_2O_3–35GeO_2–35SiO_2 before (lower curve) and after (upper curve) thermal treatment at the crystallization temperature of 690 °C for 15 min.

3.2. Nanophase optical absorption

Samples of glass with composition 7.5Li_2O–2.5Na_2O–20Ga_2O_3–35GeO_2–35SiO_2, both untreated and treated at the crystallization temperature of 690 °C for 15 min, are optically transparent over the whole visible spectrum, and show a rapid increase in absorption coefficient α(E) with photon energy *E* in the UV region (Fig. 3). No absorption edge is however observed, up to 6.4 eV, in a Ga-free reference sample. The

absorption edge in Ga-containing samples follows the exponential behaviour of the Urbach tail at the onset of band-to-band electronic transitions [28], [29], [30]. The spectral position is consistent in both cases with band-gap energy values of Ga-oxide phases, which are reported to range from 4.2 to 5.1 eV [31], [32], [33], [34], [35], [36], [37], [38], [39], and thus reflects the presence of Ga-containing nanophases in both materials. The spectral differences upon nanocrystallization in Fig. 3, however, suggest the occurrence of important structural and/or compositional modifications. The differences arise from (i) the mean spectral position of the edge, (ii) the temperature dependence of the spectral position, (iii) the slope of the edge, and (iv) the temperature dependence of the edge slope.

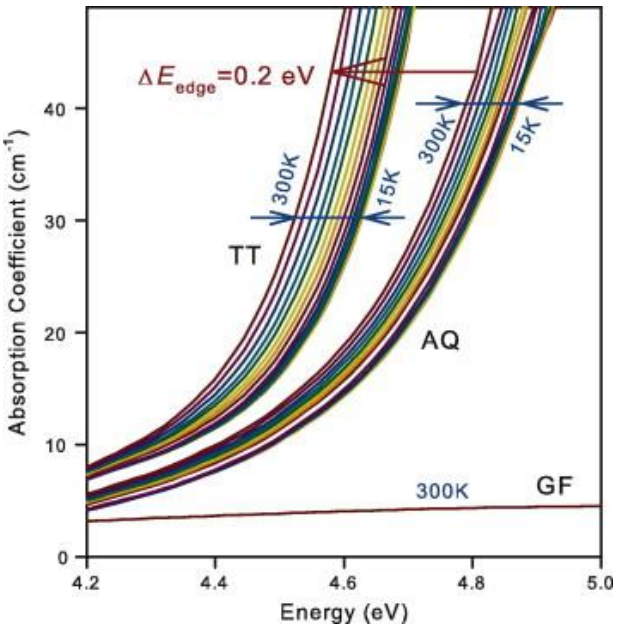

Fig. 3. Optical absorption spectra of as-quenched glass (AQ) and thermally treated nanostructured glass (TT) at different temperatures from 15 to 300 K in steps of about 25 K. The room temperature spectrum of Ga-free material (GF) is shown as a reference.

The high-energy shift of the absorption edge of as-quenched glass with respect to the glass with Ga_2O_3 nanocrystals suggests that native nanoheterogeneities could consist of a mixed silicate or germanate Ga-oxide. In fact, both SiO_2 and GeO_2 have an optical gap wider than any Ga_2O_3 phases and can contribute to the formation of Ga-containing amorphous phases with optical gaps wider than in crystalline Ga_2O_3.

More detailed information can be extracted by analyzing the thermal dependence of slope and spectral shift. In this spectral region, the absorption coefficient α(E) increases as exp(E/EU), where EU is the Urbach energy, which is related to the spread of localized energy levels at the edges of the energy gap [28]. The more gradual edge slope in as-quenched material—described by greater EU values—manifests a broader energy distribution of disorder-induced localized states. Furthermore, the slope and spectral position are much less dependent on the temperature. This fact points to static structural disorder as the main source of edge broadening of native heterogeneities. This can be quantified by calculating $E_U(T)$ from the fit of the exponential absorption edge, and analyzing the temperature dependence of $E_U(T)$. The data in Fig. 4 show that $E_U(T)$ is much larger in as-quenched glass. However, the *T*-dependence is less pronounced than in crystallized material. The data can be further analyzed as the result of contributions from *T*-dependent dynamic disorder and *T*-independent static disorder according to [28], [29], [30]:(1)

$$E_U(T)=(h\nu/\sigma)\coth(h\nu/2kT)+h\nu X/2\sigma \qquad (1),$$

where hν is the characteristic cut-off phonon energy in the Einstein model of phonon-dependent properties, σ is a dimensionless parameter which represents a correction to hν to account for the real distribution of density of states in the phonon spectrum, and *X* is the static disorder parameter proportional to the mean-square deviation $\sigma^2(x)$ of the distribution of relative atomic positions and normalized by the zero point square uncertainty $\delta^2 x_0$ (with $\delta(x_0)$ of the order of 0.1 Å) [29]. In treated material, σ is of the order of unity, as in other simple compounds [28], [29], [30], [40], whereas it is an order of magnitude greater in as-quenched glass, suggesting a wide energy distribution of the real phonon spectrum, as in amorphous multicomponent oxides. Analogously, we find that *X* is much larger in as-quenched glass than in nanocrystallized material, in which *X* is comparable with values found in topologically ordered systems with short-range disorder induced by coordination defects [28], [29], [30], [40]. The very large *X* value in as-quenched glass (similar to values in amorphous mixed oxides and highly defective crystals with complex composition [41], [42]) indicates that native amorphous nanoheterogeneities are characterized by structural disorder with a distribution of relative atomic positions comparable with the bond lengths. This

situation is expected in multinary amorphous compounds, in which topological disorder is accompanied by site-to-site variations of coordination number under the action of coexistent network modifier and network former agents. Therefore, from the *X* and σ values we can argue that native nanoheterogeneities possess a multinary composition and, as a consequence, the treatment-induced nanophase modification is unlikely to involve crystallization of an amorphous oxide, but rather a change of composition. The analysis of absorption edge shift and change of refractive index gives further insight in this regard.

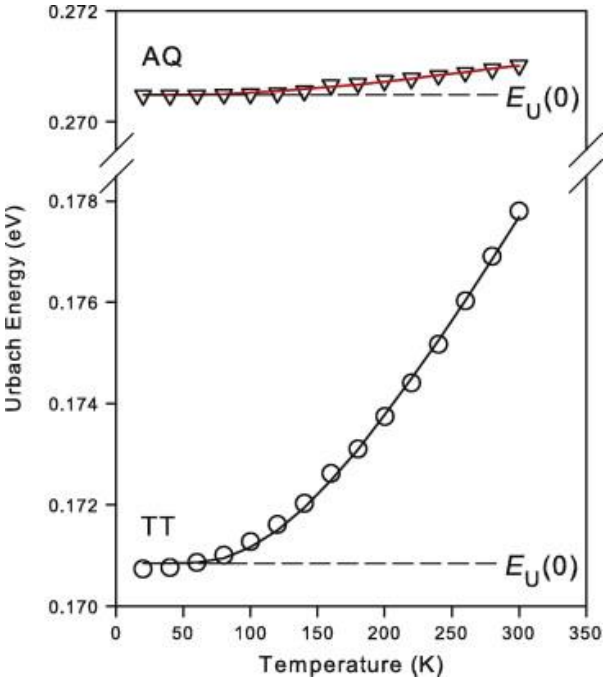

Fig. 4. Temperature variation of Urbach energy from the fit of the optical absorption edge according to Eq. (1), in as-quenched (AQ) and thermally treated (TT) Ga-containing germanosilicates. The definition of the limit $E_U(0)$ value reported in Table 2 is also shown.

3.3. Refractive index, composition and nanostructures

Confirmation that the observed shift of the absorption edge actually reflects a change in the onset of band-to-band transitions of different nanostructures comes from refractive index measurements. Refractive index is in fact expected to be sensibly affected by modifications of the intrinsic absorption spectrum through the Kramers–Kronig relations. Accordingly, we find that the refractive index *n* (measured at 633 nm with an uncertainty of $\pm 10^{-3}$) is progressively larger moving from Ga-free reference glass to as-quenched

Ga-containing glass, up to the largest value in nanocrystallized sample (see Table 2). The difference between Ga-free and Ga-containing glass reflects the introduction of an additional oxide component in the glass composition. By contrast, no change of the overall material composition can be invoked to explain the difference of refractive index (about 0.8×10^{-2}) between treated and untreated samples. The analysis of the refractive index change can give some insight into the evolution of the native nanoheterogeneities towards γ-Ga_2O_3 nanocrystals. In particular, we can analyze the relation between the refractive index change and the shift of about 0.2 eV of the absorption edge (Fig. 3 and Eedge values in Table 2). The analysis of this relation is, however, not completely straightforward. On the one hand, after nanocrystallization, the Eedge is quite consistent with the onset of band-to-band intrinsic transitions in crystalline Ga_2O_3 [31], [39], and the observed absorption edge can be reliably ascribed to the optical gap of the γ-Ga_2O_3 crystalline nanophase identified in XRD and TEM analysis. On the other hand, the absorption edge in as-quenched glass cannot be directly ascribed to nanoheterogeneities. In fact, oxide-in-oxide amorphous nanoheterogeneities in amorphous matrix could in principle possess optical and electronic properties without clear-cut differences with respect to the rest of the glass, and the observed absorption edge could indeed arise from band-to-band transitions of the whole Ga-containing glass, with only minor effects deriving from composition heterogeneity. However, the available data of *n vs* Eg—analyzed for a wide variety of oxides by Duffy and other researchers [43], [44]—allows us to disentangle the question. As a matter of fact, the refractive index *n* in the transparency region and the optical gap Eg of oxides were found to follow Duffy's relation [43], [44]:

$$Eg \propto (1-(n^2-1)/(n^2+2))^2 \qquad (2),$$

which describes, according to the Kramers–Kronig relationships, the dependence of material refractivity on the spectral distribution of the optical absorption and, specifically, on the main intrinsic absorption contribution whose threshold corresponds to the material band-gap energy. In Fig. 5 we report the dependence predicted by Eq. (2), quantitatively adjusted by a multiplicative factor so as to match (within an uncertainty of about 1%) the literature values of optical energy gap and refractive index in the visible region

of SiO_2 and Ga_2O_3 taken as a reference. According to this relation, the refractive index we register in Ga-free glass suggests an energy gap wider than 7.5 eV, outside the spectral range accessible in our experiment, consistent with the lack of absorption edge in the collected spectrum (GF curve in Fig. 3). By contrast, both as-quenched and nanocrystallized Ga-containing material show an absorption edge below 5 eV, notwithstanding the measured refractive index is not very far from the Ga-free glass value. In particular, hypothetical homogeneous oxides with refractive index equal to the value observed in Ga-containing as-quenched glass are expected to possess an optical gap energy not lower than 7 eV (horizontal dashed arrow in Fig. 5), contrary to experiment. This fact is evidence of phase separation with formation of a segregated oxide with an optical absorption edge which dominates the spectral region of transparency of the remaining matrix, and with a refractive index value which contributes only a minor part (approximately corresponding to the volume fraction of the segregated phase) to the refractive index of the whole material. More precisely, as usually encountered in nanostructured glasses [6], the resulting refractive index is given by the Maxwell–Garnett expression:

$$(n^2-n_g^2)/(n_2+2\,n_g^2)=f_v((n_n^2-n_g^2)/(n_n^2+2n_g^2)) \qquad (3)$$

where n, n_n and n_g are the refractive index values of material, segregated nanophase and remaining glass matrix, respectively, and f_v is the volume fraction. From Duffy's curve in Fig. 5, we can obtain an estimation of the refractive index of the segregated phases in the two samples, based on the spectral position of the observed absorption edge (vertical arrows in Fig. 5) and assuming the refractive index of γ-Ga_2O_3 equal, within the accuracy of the analysis, to the reference value of β-Ga_2O_3 [37], [44], [45] (no *n*-data is in fact available for the γ-phase). We find that the edge shift of about 0.2 eV (Fig. 3 and Table 2) implies a refractive index difference of 3.2×10^{-2} between γ-Ga_2O_3 nanophase and amorphous nanoheterogeneities, and indicates that native nanophase is a Ga-containing mixed oxide quite close to the composition of pure Ga-oxide. More detailed indication can be extracted by analyzing the estimated refractive index of the nanophase according to Eq. (3). We report in Fig. 6 the expected dependence $n_g(f_v)$ of the glass matrix refractive index in as-quenched material (dashed curve) as a function of the volume fraction of

nanoheterogeneities at fixed refractive index values *n* and n_n of material and nanophase (*n* = 1.6266 from direct measurement of as-quenched material, and n_n = 1.9250 from optical gap energy Eg = 4.7 eV through Duffy's relation in Fig. 5). Taking into account that the molar concentration of Ga-oxide is 20%, the expected nanophase volume fraction is likely larger than 0.2, as one can argue from the larger molar volume of Ga-oxides (about 29–31 $cm^3\ mol^{-1}$ [44], [46]) with respect to Ge- and Si-oxides (28.3 and 27.3 $cm^3\ mol^{-1}$, respectively). Therefore, for volume fraction of nanoheterogeneities larger than 20%, the analysis in Fig. 6 of the native glass matrix points to ng values smaller than in Ga-free glass, as expected in a SiO_2-rich matrix. In other words, the glass matrix of as-quenched glass appears partially depleted in GeO_2 content and, consequently, the native nanoheterogeneities should consist of some kind of GeO_2-enriched amorphous Ga-oxide. This analysis is consistent with the high-energy shift of the absorption edge with respect to Ga-oxide, and it is also quite reasonable for the similarity between Ga and Ge covalent radii (126 and 122 pm, respectively). Therefore, the secondary phase separation and nanocrystallization of γ-Ga_2O_3 turns out to comprise the segregation of Ga-oxide from a mixed Ge/Ga-oxide. Further insight into the mechanisms involved can be obtained by joining the analysis of the optical data with an investigation of the modification of the dielectric response.

Material	n_{633}	E_{edge}	$E_U(0)$	hν	*X*	σ
AQ	1.627	4.7	270.5	31	863	50
TT	1.635	4.5	170.9	36	31	3.4
GF	1.572	>6.4	–	–	–	–

Table 2. Optical data. Refractive index n633 at 633 nm (±10-3), energy Eedge of the optical absorption edge in eV (±0.5 eV), low T limit EU(0) of the Urbach energy in meV (±0.3 meV), Einstein cut-off phonon energy hν in meV (±1 meV), a dimensional disorder parameter X and a phonon correction parameter σ in Eq. (1) (±1%).

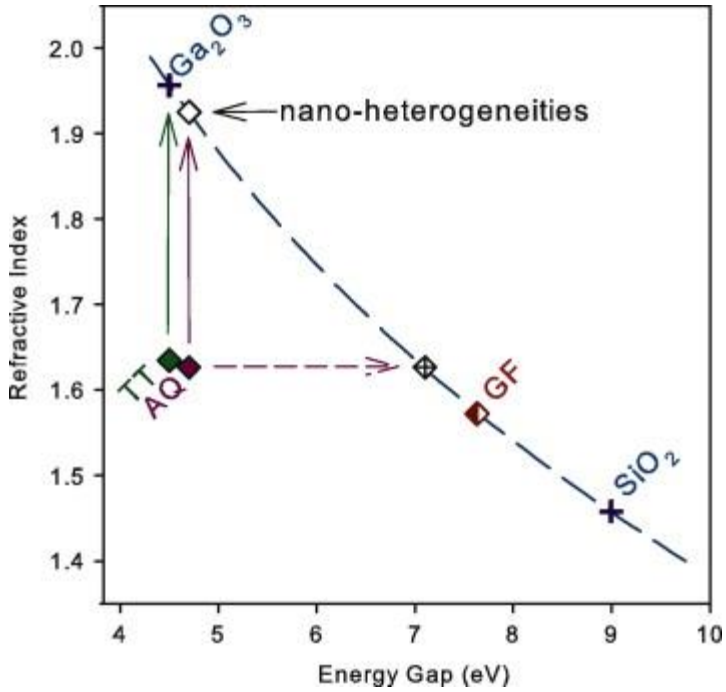

Fig. 5. Measured (filled symbols) and calculated (open symbols) values of refractive index (at 633 nm) and energy gap (from the spectral position of the optical absorption edge) of Ga-free glass (GF), Ga-containing as-quenched glass (AQ), and thermally treated nanocrystallized Ga-containing glass (TT). Calculated values of the energy gap (refractive index) are derived according to Duffy's relation in Eq. (2) from the measured value of refractive index (energy gap) as indicated by dashed (continuous) arrows. Duffy's relation in Eq. (2)—multiplied by a factor to fit reference values of SiO_2 and Ga_2O_3 from literature (crosses)—is reported as a dashed line.

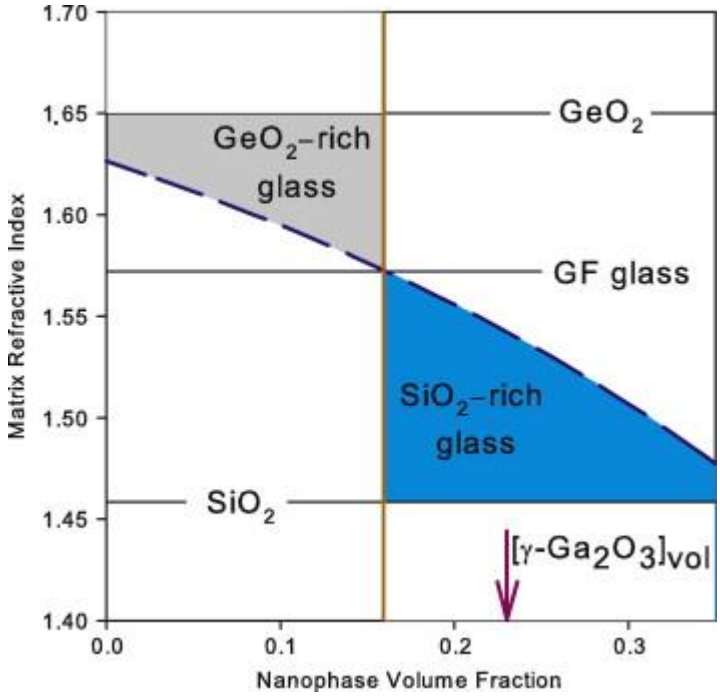

Fig. 6. Refractive index ng (dashed line) of the glass matrix in as-quenched material, calculated according to Eq. (3) as a function of the nanophase volume fraction, starting from the refractive index values n and nn of material and nanophase (n = 1.6266 from direct measurement of as-quenched material, and nn=1.9250 from optical gap energy, see Fig. 5). The limit situations of pure GeO_2 and SiO_2 glasses are also shown, as well as the reference data of Ga-free glass with balanced molar concentration of GeO_2 and SiO_2. The calculated volume fraction of 20 mol.% of crystallized γ-Ga_2O_3 from density and molar mass data is reported as a reference on the x-axis.

3.4. Complex dielectric function analysis

Drastic rearrangements of mean coordination structure are expected as a result of the secondary phase separation and the subsequent transformation of the amorphous network into a matrix with a crystalline nanophase. In particular, because of the segregation of Ga from glass to nanocrystals, relevant changes may involve Ga^{3+} coordination (with the formation of a mainly octahedral coordination), alkali ions (removed from a charge compensator role at Ga sites) and non-bridging-oxygen (NBO) groups (mainly as coordination defects in the final alkali-modified glass matrix and on the interphase). The analysis of the dielectric response can give some insight into these mechanisms, providing information on the change of molar polarization. Fig. 7 shows the results of complex impedance measurements on Ga-containing and Ga-

free glasses, reported as frequency dependence of the electric conductivity σ(ν) (Fig. 7a) and relative electric permittivity ∈r(ν) (Fig. 7b). Both ∈r(ν) and σ(ν) show the typical dependences observed in dielectric glasses. In fact, σ(ν) follows a power law according to the relation $\sigma=\sigma_{dc}+k\nu^s$, where σ_{dc} is the DC conductivity, *k* is a constant, *s* is an exponent lower than 1, and $k\nu^s$ the frequency-dependent part σ_{ac} of the electric conductivity [1], [47]. In fact, we do not register any appreciable contribution from σdc. Hence, since σ_{ac} is the only term in σ(ν), the imaginary part ∈″ of the dielectric function can be calculated as $\in\sigma_{ac}/2\pi\nu\in_0$ from Fig. 7a, whereas the real part ∈′ is directly given by ∈r in Fig. 7b.

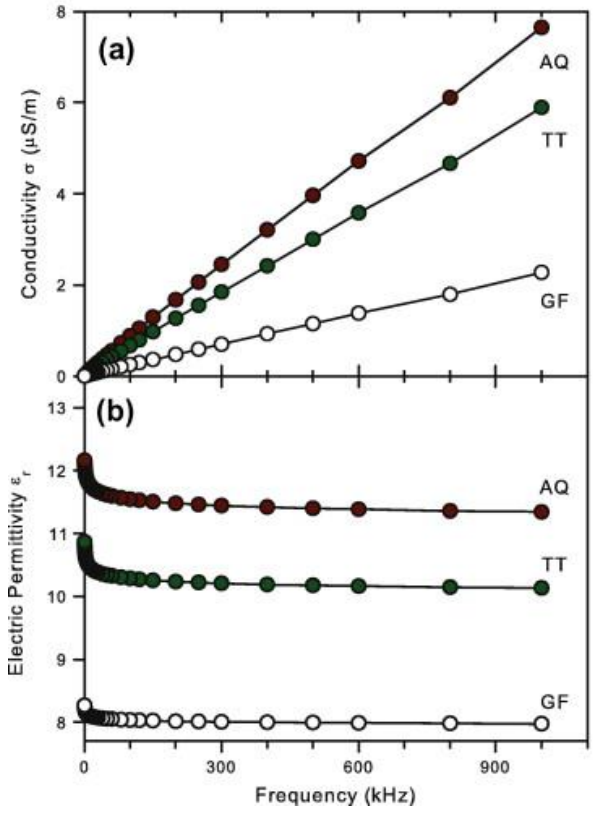

Fig. 7. Electric conductivity (a) and relative electric permittivity (b) of Ga-containing glasses before (AQ) and after (TT) thermal treatment of nanocrystallization, compared with a reference Ga-free sample (GF).

The Cole–Cole plots in Fig. 8 show that ∈′ and ∈″ approximate a linear relationship at increasing frequency, as expected in dielectric materials, with an intercept ∈′=∈int at ∈″=0 [1]. The intermediate dielectric constant ∈int represents the response of the dielectric material in the intermediate-frequency range dominated by intrinsic mechanisms of electronic and ionic lattice polarization. These mechanisms appear

almost instantaneous up to frequencies of the order of a few GHz, and give rise to a purely real contribution to the dielectric function [1], [47]. The data in Fig. 8 instead deviate from linearity at low frequency, reflecting the presence of contributions of dielectric loss from slow polarization responses, e.g. from hopping charge carriers of electronic or ionic nature or defect-like permanent dipoles of vacancy–interstitial pairs. The estimated ∈int value, disregarding low-frequency mechanisms, is therefore related to polarization contributions—both electronic and ionic—of the coordination structure [1].

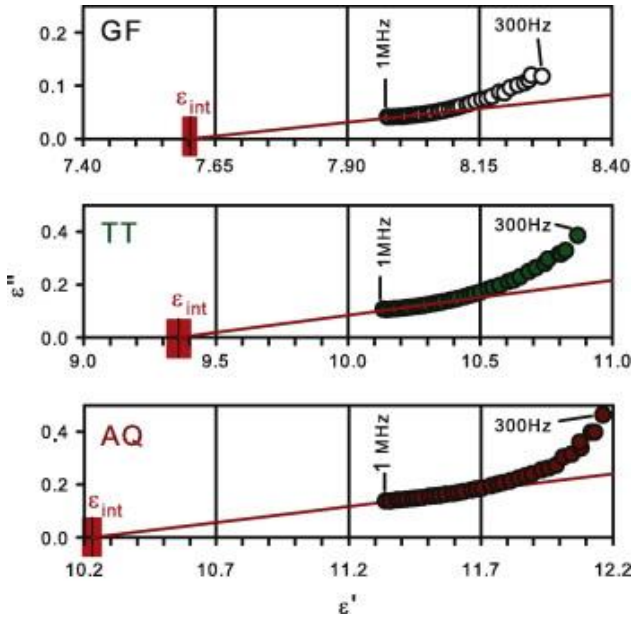

Fig. 8. Cole–Cole plot of the real and imaginary part ∈′ and ∈″ of the dielectric function in Ga-containing glass before (AQ) and after (TT) thermal treatment of nanocrystallization, compared with Ga-free reference material (GF). Lines are the results of linear regression of data from 40 kHz to 1 MHz to determine high-frequency interpolation of the intermediate electric permittivity ∈int; the width of the rectangular areas at the intercept points is twice the standard error on the intercept position.

Fig. 8 shows clear-cut changes of ∈int after addition of Ga-oxide and also after thermally induced nanocrystallization. Specifically, gallium addition causes ∈int to change from 7.6 to 10.2, as expected by the increase in mean electron density. By contrast, nanocrystallization instead lowers the electric permittivity ∈int, which decreases from 10.2 to 9.3. Such a change is opposite to the refractive index change, which slightly increases as a result of nanocrystallization (see Table 2). This result points to the

distinct effects of nanocrystallization on the electronic and ionic polarization mechanisms. The former mechanism is by far the main source of the dielectric response described by the dielectric function $\epsilon\infty=n^2$ at the optical frequencies of refractive index measurements. It arises from electric-field-induced deformation of the negative charge density around the positive atomic nucleus. The latter mechanism—dependent on electric-field-induced modifications of relative positions of anions and cations in the structure—instead contributes, together with the electronic polarization, to the dielectric response described by ϵint at much lower frequency. Therefore, the analysis of $\epsilon\infty$ and ϵint can provide a deeper insight into the coordination changes caused by nanocrystallization. To do this we have to disentangle the contributions of electronic and ionic polarization to the molar polarization.

To analyze the different polarization contributions and to recognize the role of specific structural components inside the mixed oxides, we introduce the molar polarizability $\alpha_M=(4\pi/3)NA\alpha_m$, where NA is the Avogadro number and α_m is the molecular polarizability (in m^3 or $Å^3$) connected with the polarizability α (in $C^2\,N^{-1}\,m$) through the relation $\alpha_m=\alpha/4\pi\epsilon_0$. With this position, the dielectric/refractive response of the material can be related to the polarization mechanisms inside the solid at intermediate/optical frequencies through, respectively, the Clausius–Mossotti/Lorentz–Lorenz relation [1]:

$$\alpha_M=V_M\,(\epsilon-1)/(\epsilon+2) \qquad (4)$$

where V_M is the molar volume of the material (Table 1) and ϵ takes the value ϵint in the intermediate-frequency range, and the value $\epsilon\infty=n^2$ at optical frequencies. The molar polarizability so defined (in $m^3\,mol^{-1}$ or $cm^3\,mol^{-1}$) turns out to be additive with respect to concomitant polarization mechanisms. Specifically, electronic and ionic polarization can be described by the molar polarizability contributions α_M^e and α_M^i, respectively. As a result, taking into account that both α_M^e and α_M^i contribute at intermediate frequency, whereas only α_M^e is relevant in determining the refractive response, Eq. (4) can be rewritten as:

$$\alpha_M=VM(\epsilon int-1)/(\epsilon int+2)=\alpha_M^e+\alpha_M^i=V_M((n^2-1)/(n^2+2))+\alpha_M^i \qquad (5)$$

On the right-hand side of Eq. (5), refractive index data (from Table 2) are used to estimate α_M^e, which is then subtracted from αM (obtained from ∈int data of Fig. 8) to calculate αMi (e.g. [1], [47]). We report in Table3 the values of α_M,α_M^e and α_M^i obtained in this way.

Empty Cell	**GF**	**AQ**	**TT**	Empty Cell	**Ga_2O_3**
α_M	16.6	20.4	19.9	(17.7)	22.0
α_M^e	7.93	9.59	9.69	(9.40)	15.3
α_M^i	8.63	10.8	10.2	(8.24)	6.70

Table 3. Total molar polarization α_M, electronic polarization α_M^e and ionic polarization α_M^i of Ga-free reference glass (GF), as-quenched glass (AQ) and thermally treated nanocrystallized material (TT). Reference values of Ga_2O_3 from the literature data are also shown, and (in parenthesis) values calculated in additive approximation from GF and Ga_2O_3 values weighted by the molar concentration of glass matrix and nanophase, respectively, in the TT sample. All values are in $cm^3\ mol^{-1}$ with an uncertainty of about 0.5%.

Most evident outcome in Table 3 is the opposite sign of the electronic and ionic polarizability changes, with a significantly larger decrease in ionic contribution with respect to the smaller increase in the electronic one. To analyze this result, it is useful to compare the data with the expected response from the glass-only matrix and from the crystalline phase alone, as well as with the simple linear combination of these forms. We can estimate such a response from the results on Ga-free glass and the values of Ga_2O_3 polarizability reported in the literature [45], [48]. In fact, on the one hand the molar polarizability of Ga-free material represents a good estimation of the response of all electronic configurations participating in the alkali-germanosilicate matrix of Ga-containing nanocrystallized material. On the other hand, studies on several Ga-containing mixed oxides showed that the dielectric polarizability of Ga_2O_3 component, even distributed in multinary compounds such as rare earth gallium garnets, keeps the value 8.8 $Å^3$, as in pure Ga-oxide [45], [48], [49], with a variability of 2% at most [48]. As far as the response of the nanostructured

system can be described as the result of additive polarizabilities of distinct phases (weighted by the molar concentrations), both ionic and electronic molar polarizability—and the total molar polarizability—can be expressed as:

$$\alpha_M^{e,i}=[x]\alpha_M^{e,i}(Ga_2O_3)+[1-x]\ \alpha_M^{e,i}\ (\text{Ga-free}) \qquad (6),$$

where x=0.20 is the molar concentration of Ga-oxide in the material. Values calculated through this expression are reported in Table 3 (in parentheses). Interestingly, they are significantly smaller than the experimental ones (well above uncertainty), with only α_M^e approaching much more than the other contributions the measured value, even though largely outside uncertainty.

3.5. Polarizability and coordination changes

Information on the nanostructural sources of changes in the dielectric and refractive response can be extracted by considering not only α_M^e and α_M^i (positive and negative, respectively, as a result of nanostructuring), but also the discrepancy between measured quantities and values calculated from the additive approximation. As regards α_M^e, the main factor that should be considered is the change in anion polarizability. In fact, although the electronic polarizability reflects the response of the electronic configuration of each ion in the structure, the polarizability of O^{2-} ions usually largely overcomes the polarizability of cations in oxides. The free-ion *m* values calculated by Pauling for Si^{4+}, Ge^{4+}, Li^+, Na^+ and Ga^{3+} are 0.033, 0.143, 0.029, 0.181 and 0.195 Å^3, respectively, i.e. an order of magnitude smaller than the O^{2-} polarizability in SiO_2, GeO_2 and Ga_2O_3, which have *m* values of 1.401, 1.720 and 1.732 Å^3, respectively [2]. Therefore, the positive αMe could be related to a change in mean O^{2-} polarizability. Specifically, αMe could in principle be related to the change in the mean coordination of Ga ions, since oxygen ions are expected to possess larger polarizability in Ga–O bonds of octahedral Ga sites than in bonds of tetrahedral sites. However, the possible O^{2-} values are quite similar in the present compound (especially in Ge and Ga sites) and the differences can hardly justify the observed increase of αMe. In fact, taking O^{2-} = 1.732 Å^3 as the mean O^{2-} polarizability in Ga_2O_3 and supposing that in tetrahedral Ga sites

O^{2-} = 1.720 Å^3 as in Ge sites (probably an underestimation), the increase of O^{2-} polarizability would be less than 0.7%. Hence, even in the unrealistic case of full change of coordination from tetrahedral to octahedral upon Ga-oxide crystallization, the expected increase of polarizability from all O^{2-} ions belonging to the Ga_2O_3 component could only account for one-fifth of the observed α_M^e. Therefore, other concurrent mechanisms of change of the mean oxygen polarization are necessarily the main source of the change in refractive index. Since the process of nanocrystallization involves the formation of a large interphase between glass matrix and nanocrystals—with quite different mean coordination structure—the formation of a high concentration of NBO sites can be the source of a relevant change of the mean O^{2-} polarizability. In fact, the expected increase of O^{2-} from a X–O–X bond (with X = Ga, Ge) to NBOs is as large as 50%, according to an estimated value O^{2-} = 2.59 Å^3 for NBOs in sodium silicate glass [1]. The surface-to-volume ratio is quite large in the nanocrystallized glass and, taking a mean nanocrystal size of 6 nm, the fraction of coordination units at the interphase is estimated to be about 30% of the total number of units belonging to the nanophase. In such a situation, it is sufficient that 1/4 of the oxygen ions at the interphase belong to NBO groups, because the expected enhancement of α_M^e can match the experimental value of 0.1 cm^3 mol^{-1}.

The possible origin of the even greater but opposite modification of ionic polarizability α_M^i must instead be looked for in the change of coordination cages around the cations, since α_M^i describes the deformations induced by the electric field on the relative positions of the anions and cations. No relevant change is, however, expected in the ionic polarizability of SiO_4 and GeO_4 tetrahedra, whose structure can be considered stable with respect to the observed phase separation. Modifications of αMi can only be ascribed to changes in the structural units centered in Ga^{3+} sites and in M^+ alkali cations. Both kinds of sites can in fact undergo modification of the respective coordination. Ga sites admit both tetrahedral and octahedral oxygen cages, whereas M^+ alkali ions can possess a variety of oxygen cages, with quite large coordination number from 5 to 8, as observed in other alkali silicates by extended X-ray absorption fine structure (EXAFS) and molecular dynamics (MD) simulation [50], [51]. The M^+-coordinated oxygens can belong either to Si–O–Si and Ge–O–Ge bonds, or to ionic groups which contribute to sharing the electron charge of the alkali ion, such as NBOs (in O–M^+ groups) and GaO_4 tetrahedra (in GaO_4–M^+ complexes). This

is likely the initial situation in as-quenched glass, in which Ga oxide takes part in the amorphous heterogeneities composed of some mixed alkali gallate/germanate phase, as suggested by optical absorption and refractive index (Fig. 5, Fig. 6, Section 3.3). However, after nanocrystallization, Ga oxide is mainly confined in nanocrystals—without any need of charge compensation from alkali ions—and alkali ions can mainly coordinate with NBOs in the matrix and on the interphase. The ionic polarizability of M^+ sites is expected to be lowered by removing Ga-coordinated oxygens from their average shell of coordination, because the bond strength in a GaO_4 tetrahedron is weaker than in a $O–M^+$ bond of NBOs. In sodium aluminosilicates, as a reference, αMi is lower in $O–M^+$ bonds than in $AlO_4–M^+$ groups by approximately 30%, with a difference αNai of about 1.5 Å^3. We can use this value to estimate the order of magnitude of the expected αMi in the present compound. If we suppose that the lack of polarizability contribution from $GaO_4–M^+$ groups upon nanocrystallization accounts even for only half the molar concentration of alkali ions in our compound (supposing, for instance, the occurrence of some amount of Ga ions in the matrix even after nanocrystallization), we obtain α_M^i =0.4 cm^3 mol^{-1}, a value that matches the experiments (Table 3). This estimate also suggests that modifications of mean Ga coordination probably make only minor contributions not only to the molar electronic polarizability, but also to the ionic one. Importantly, according to this analysis, contributions of polarizability from $O–M^+$ bonds are larger than contributions from M^+ sites interacting only with Si–O–Si and Ge–O–Ge bonds (predominant in Ga-free glass). This fact explains why the molar polarizability in the treated sample exceeds the value calculated by the additive rule using data for Ga-free glass and Ga_2O_3.

Finally, in order to directly verify the occurrence of NBOs and to obtain a confirmation of some modification of their concentration upon nanocrystallization, we have looked for evidence of NBOs in the photoluminescence spectrum excited at 633 nm. The collected spectra (Fig. 9) show the typical red luminescence of NBOs in oxides [17], [52], [53], [54], [55]. Importantly, the effect of Ga addition in promoting the formation of NBOs is evident. In fact, the photoluminescence band in Ga-free glass is almost undetectable compared with Ga-containing as-quenched glass, which is more than one order of magnitude more intense. The light emission intensity further increases upon crystallization, consistently with the analysis of the dielectric response and refractive index change. It should be noted here that the significant

increase in NBO luminescence in nanocrystallized glass cannot be ascribed to the coordination network of the crystalline nanophase, since Ga_2O_3 nanopowders and films, and even single crystals, do not show such an emission, which rather is typical of mixed oxide glasses with network modifier ions.

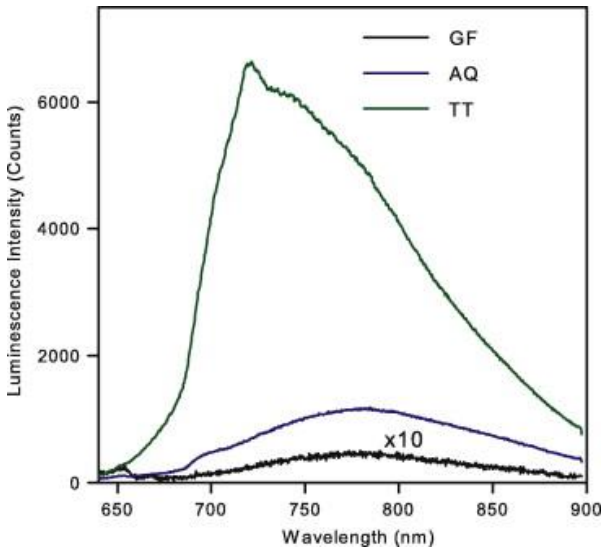

Fig. 9. Photoluminescence spectra excited at 633 nm of Ga-modified germanosilicates before and after thermal treatment, compared with Ga-free glass.

4. Conclusions

Analysis of the optical and dielectric response in Ga-modified germanosilicate glass indicates that it is possible to use Ga addition to change the dielectric function and refractive index of glass through post-synthesis growth of γ-Ga_2O_3 nanocrystals. This study of changes in the optical absorption edge, refractive index and electric permittivity gives unprecedented insight into the process of secondary phase separation and nanocrystallization, clarifying that initial heterogeneities include Ge-oxide and alkali ions inside an amorphous Ga-oxide phase. Analysis of the contributions of polarizability to the changes in dielectric and refractive response points to a key role of NBO generation during nanocrystallization. Finally, understanding of the mechanisms involved permits analogous strategies in different oxides to be conceived.

Acknowledgements

This work has been supported by the Ministry of Education and Science of the Russian Federation under Grant No. 11.G34.31.0027, by Cariplo Foundation, Italy, under Project No. 2012-0920, and by Grant MK-1398.2014.3.

References

[1] Hsieh CH, Jain H, Kamitsos EI. J Appl Phys 1996;80:1704–12.
[2] Dimitrov V, Komatsu T. J Univ Chem Technol Metall 2010;45:219–50.
[3] Niay P, Douay M, Bernage P, Xie WX, Leconte B, Ramecourt D, et al. Opt Mater 1999;11:115–29.
[4] Canning J, Sommer K, Englund M, Huntington S. Adv Mater 2001;13:970–3.
[5] Chiodini N, Ghidini S, Paleari A. Phys Rev B 2001;64:073102.
[6] Chiodini N, Paleari A, Spinolo G. Phys Rev Lett 2003;90:055507.
[7] Paleari A, Franchina E, Chiodini N, Lauria A, Bricchi E, Kazansky PG. Appl Phys Lett 2006;88:131912.
[8] Zhang J, Gecevic˘ius M, Beresna M, Kazansky PG. Paper CTh5D.9 in CLEO: 2013, OSA Technical Digest (online) Optical Society of America; 2013.
[9] Royon A, Bourhis K, Bellec M, Papon G, Bousquet B, Deshayes Y, et al. Adv Mater 2010;22:5282–6.
[10] Chiodini N, Lauria A, Lorenzi R, Brovelli S, Meinardi F, Paleari A. Chem Mater 2012:24677–81.
[11] Brovelli S, Chiodini N, Lorenzi R, Lauria A, Romagnoli M, Paleari A. Nat Commun 2012;3:690. http://dx.doi.org/10.1038/ncomms1683.
[12] Sigaev VN, Golubev NV, Ignat'eva ES, Savinkov VI, Campione M, Lorenzi R, et al. Nanotechnology 2012;23:015708.
[13] Nagaraja L, De Souza RA, Samuelis D, Valov I, Brger A, Janek J, et al. Nat Mater 2008;7:391–8.
[14] Zhou S, Jiang N, Dong H, Zeng H, Hao J, Qiu J. Nanotechnology 2008;19:015702.
[15] Zhou S, Jiang N, Wu B, Hao J, Qiu J. Adv Funct Mater 2009;19:2081–8.
[16] Samson BN, Pinckney LR, Wang J, Beall GH, Borrelli NF. Opt Lett 2002;27:1309–11.
[17] Mashinsky VM, Karatun NM, Bogatyrev VA, Sigaev VN, Golubev NV, Ignat'eva ES, et al. Microsc Microanal 2012;18:259–65.
[18] Lotarev SV, Lipatiev AS, Golubev NV, Ignat'eva ES, Malashkevich GE, Mudryi AV, et al. Opt Lett 2013;38:492–4.
[19] Sigaev VN, Golubev NV, Ignat'eva ES, Champagnon B, Vouagner D, Nardou E, et al. Nanoscale 2013;5:299–306.
[20] Sigaev VN, Golubev NV, Ignat'eva ES, Paleari A, Lorenzi R. Nanoscale 2014;6:1763–74.
[21] Tanaka K, Mukai T, Ishihara T, Hirao K, Soga N, Sogo S, et al. J Am Ceram Soc 1993;76:2839–45.
[22] Yamaguchi I, Tanaka K, Hirao K, Soga N. J Mater Sci 1996;31:3541–7.
[23] Park BJ, Chang HJ, KKim DH. Appl Phys Lett 2004;85:6353–5.
[24] Zachariasen WH. J Am Chem Soc 1932;54:3841–51.
[25] Ash JT, Grandinetti PJ. Magn Reson Chem 2006;44:823–31.
[26] O'Dell LA, Savin SLP, Chadwick AV, Smith ME. Appl Magn Reason 2007;32:527–46.
[27] Middlemiss DS, Blanc F, Pickard CJ, Grey CP. J Magn Reason 2010;204:1–10.
[28] Saito K, Ikushima A. Phys Rev B 2000;62:8584–7.
[29] Cody GD, Tiedje T, Abeles B, Brooks B, Goldstein Y. Phys Rev Lett 1981;47:1480–3.
[30] Paleari A, Meinardi F, Brovelli S, Lauria A, Lorenzi R, Chiodini N. Appl Phys Lett 2007;91:141913.
[31] Hao J, Cocivera M. J Phys D 2002;35:433–8.
[32] Rebien M, Henrion W, Hong M, Mannaerts JP, Fleischer M. Appl Phys Lett 2002;81:250–2.
[33] Passlack M, Schubert EF, Hobson WS, Hong M, Moriya N, Chu SNG, et al. J Appl Phys 1995;77:686–93.
[34] Orita M, Ohta H, Hirano M, Hosono H. Appl Phys Lett 2000;77:4166–8.

[35] Kim H-G, Kim W-T. J Appl Phys 1987;62:2000–2.
[36] Wu P, Gao Y-M, Kershaw R, Dwight K, Wold A. Mater Res Bull 1990;25:357–63.
[37] Ortiz A, Alonso JC, Andrade E, Urbiola C. J Electrochem Soc 2001;148:F26–9.
[38] Al-Kuhaili MF, Durrani SMA, Khawaja EE. Appl Phys Lett 2003;70:4533–5.
[39] Tippins HH. Phys Rev 1965;140:A316–9.
[40] Lorenzi R, Brovelli S, Meinardi F, Lauria A, Chiodini N, Paleari A. J Non-Cryst Solids 2011:357;1838–1841.
[41] Johnson SR, Tiedje T. J Appl Phys 1995;78:5609–13.
[42] Grus M, Sikorska A. Physica B 1999;266:139–45.
[43] Duffy JA. J Solid State Chem 1986;62:145–57.
[44] Dimitrov V, Sakka S. J Appl Phys 1996;79:1736–40.
[45] Passlack M, Hunt NEJ, Schubert EF, Zydzik GJ, Hong M, Mannaerts JP, et al. Appl Phys Lett 1994;64:2715–7.
[46] Hayashi H, Huang R, Oba F, Hirayama T, Tanaka I. J Mater Res 2011;26:578–83.
[47] Jonscher AK. Nature 1977;267:673–9.
[48] Shannon RD, Subramanian MA, Allik TH, Kokta MR, Randles MH, Rossman GR. J Appl Phys 1990;67:3798–802.
[49] Hoeneisen B, Mead CA, Nicolet MA. Solid-State Electron 1971;14:1057–9.
[50] McKeown DA, Waychunas GA, Brown Jr GE. J Non-Cryst Solids 1985;74:325–48.
[51] Zirl DM, Garofalini SH. J Am Ceram Soc 1990;73:2848–56.
[52] Dragic PD, Carlson CG, Croteau A. Opt Express 2008;16:4688–97.
[53] El Mir L, Amlouk A, Barthou C, Alaya S. Mater Sci Eng C 2008;28:771–6.
[54] Skuja L. J Non-Cryst Solids 1994;179:51–69.
[55] Suzuki T, Skuja L, Kajihara K, Hirano M, Kamiya T, Hosono H. Phys Rev Lett 2003;90:186404.